

# Conformational States of a Bacterial $\alpha_2$ -Macroglobulin Resemble Those of Human Complement C3

David Neves<sup>1,2,3</sup>, Leandro F. Estrozi<sup>1,2,3</sup>, Viviana Job<sup>1,2,3</sup>, Frank Gabel<sup>1,2,3</sup>, Guy Schoehn<sup>1,2,3,4</sup>, Andréa Dessen<sup>1,2,3\*</sup>

**1** Institut de Biologie Structurale (IBS), Université Grenoble I, Grenoble, France, **2** Centre National de la Recherche Scientifique (CNRS), Grenoble, France, **3** Commissariat à l'Energie Atomique (CEA), Grenoble, France, **4** Unit for Virus Host Cell Interactions UMI 3265 (UJF-EMBL-CNRS), Grenoble, France

## Abstract

$\alpha_2$  macroglobulins ( $\alpha_2$ M) are broad-spectrum protease inhibitors that play essential roles in the innate immune system of eukaryotic species. These large, multi-domain proteins are characterized by a broad-spectrum bait region and an internal thioester, which, upon cleavage, becomes covalently associated to the target protease, allowing its entrapment by a large conformational modification. Notably,  $\alpha_2$ M are part of a larger protein superfamily that includes proteins of the complement system, such as C3, a multi-domain macromolecule which is also characterized by an internal thioester-carrying domain and whose activation represents the pivotal step in the complement cascade. Recently,  $\alpha_2$ M/C3-like genes were identified in a large number of bacterial genomes, and the *Escherichia coli*  $\alpha_2$ M homolog (ECAM) was shown to be activated by proteases. In this work, we have structurally characterized ECAM by electron microscopy and small angle scattering (SAXS) techniques. ECAM is an elongated, flexible molecule with overall similarities to C3 in its inactive form; activation by methylamine, chymotrypsin, or elastase induces a conformational modification reminiscent of the one undergone by the transformation of C3 into its active form, C3b. In addition, the proposed C-terminus of ECAM displays high flexibility and different conformations, and could be the recognition site for partner macromolecules. This work sheds light on a potential bacterial defense mechanism that mimics structural rearrangements essential for activation of the complement cascade in eukaryotes, and represents a possible novel target for the development of antibacterials.

**Citation:** Neves D, Estrozi LF, Job V, Gabel F, Schoehn G, et al. (2012) Conformational States of a Bacterial  $\alpha_2$ -Macroglobulin Resemble Those of Human Complement C3. PLoS ONE 7(4): e35384. doi:10.1371/journal.pone.0035384

**Editor:** Ivo G. Boneca, Institut Pasteur Paris, France

**Received:** November 29, 2011; **Accepted:** March 16, 2012; **Published:** April 17, 2012

**Copyright:** © 2012 Neves et al. This is an open-access article distributed under the terms of the Creative Commons Attribution License, which permits unrestricted use, distribution, and reproduction in any medium, provided the original author and source are credited.

**Funding:** This work was funded by grant DEQ20090515390 from the Fondation pour la Recherche Médicale (FRM; French Medical Research Foundation - www.frm.org). DN was supported by a fellowship from the Conselho Nacional de Desenvolvimento Científico e Tecnológico (CNPq-Brasil) and the FRM. The funders had no role in study design, data collection and analysis, decision to publish, or preparation of the manuscript.

**Competing Interests:** The authors have declared that no competing interests exist.

\* E-mail: andrea.dessen@ibs.fr

## Introduction

$\alpha_2$ -macroglobulins ( $\alpha_2$ M) are large, multi-domain and broad-spectrum protease inhibitors present in eukaryotes that play key roles in host cell protection from parasitic or bacterial attack. These proteins are characterized by a highly reactive thioester bond as well as a bait region (Fig. 1) whose sequence is recognized by a large spectrum of proteases. The rearrangement of  $\alpha_2$ M upon cleavage of the bait region traps the attacking protease in a cage-like structure, thus rendering proteases secreted by infecting microorganisms ineffective, promoting efficient microbial clearance.  $\alpha_2$ M are thus essential elements of the innate immune system [1,2].

The  $\alpha_2$ M bait region contains recognition sites for all four classes of proteases which, once physically entrapped, are impaired from reaching their substrates [2]. Human  $\alpha_2$ M, specifically, is a tetrameric 720 kDa molecule in which each 180 kDa subunit harbors an independent bait region whose cleavage induces the exposure and subsequent hydrolysis of a pre-concealed  $\beta$ -cysteinyl-glutamyl thioester bond. This generates an irreversible conformational modification causing one or two protease molecules to become entrapped within a cage-like structure [3,4,5,6,7,8]. This modification also exposes the receptor-binding domain at the C-terminus of  $\alpha_2$ M, which is subsequently recognized by cells

harboring the low density lipoprotein-related protein (LRP), allowing clearance of  $\alpha_2$ M-protease complexes [1,2,9]. Notably, the conformational change can also be induced *in vitro* through incubation of  $\alpha_2$ M with methylamine, which directly interacts with the thioester bond without altering the bait region [3,4,5,7,8,10] and thus has been used extensively in the study of different forms of  $\alpha_2$ M molecules. Small angle scattering (SAXS) studies of human  $\alpha_2$ M revealed that the molecule becomes more compact when reacted with proteases and after incubation with methylamine [11,12]. In addition, low-resolution electron microscopy data is available for  $\alpha_2$ M in both inactive and methylamine/protease-activated forms [3,4,5,6,7,8,10], and very recently, a medium resolution structure (4.3 Å) of the methylamine-activated human  $\alpha_2$ M also became available [13].

Notably,  $\alpha_2$ M are members of the same protein superfamily as components of the complement system, such as factor C3. In addition to displaying regions of considerable sequence similarity, these proteins harbor a number of homologous domains; most family members are characterized by a conserved CxEx motif (Fig. 1), which forms the internal thioester bond that must become covalently associated to target molecules in order to ensure the protein's biological activity [1,14,15,16]. The high-resolution crystal structure of the 187 kDa C3 molecule reveals that it is

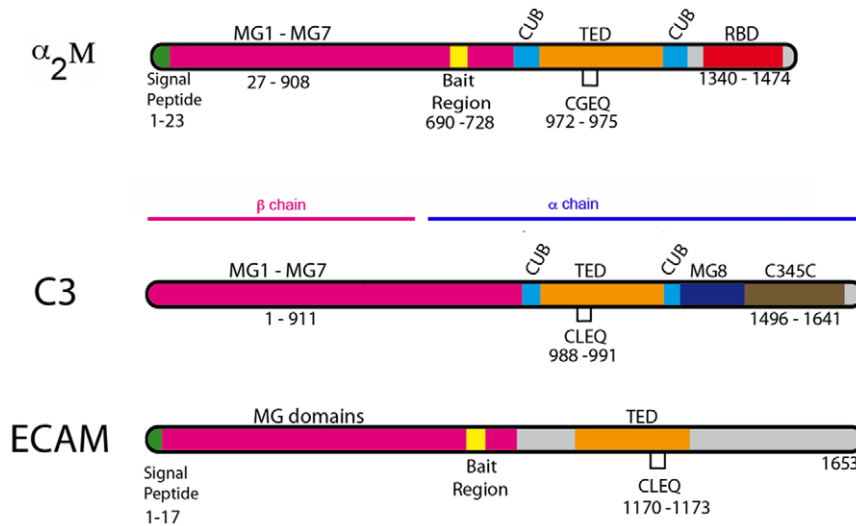


**Figure 1. Schematic representations of human  $\alpha_2$ -macroglobulin ( $\alpha_2$ M), C3 convertase (C3), and *E. coli*  $\alpha_2$ -macroglobulin (ECAM).** Domain assignments for  $\alpha_2$ M and C3 were based on their respective crystal structures [13,17]. Assignments for ECAM were performed with the JPRED server, supported by the analysis performed by Doan and Gettins [27]. Note the similarity in domain predictions, including MG and TED domains. The CLEQ sequence, a signature of the thioester bond, is present in all proteins. For simplicity, only a limited number of the domains identified or predicted for the different molecules are depicted, and only one monomer of  $\alpha_2$ M is shown. The C-terminus of ECAM displays low sequence similarity to that of C3 (Fig. S6).

doi:10.1371/journal.pone.0035384.g001

composed of two chains ( $\alpha$  and  $\beta$ ) divided into 13-domains, and that the highly reactive thioester is harbored within a protected region in the thioester-containing domain (TED) [17,18]. The pivotal step in the complement cascade is the activation of C3 by proteolysis to yield C3b, in which the TED domain relocates to a site that is 75–100 Å away from its original position in C3. This exposes the thioester to solvent, allowing it to subsequently bind covalently to antigenic surfaces [19,20,21,22,23]; solvent-exposed Cys and Gln residues of the TED domain are also a feature of the human  $\alpha_2$ M [13]. It is thus evident that molecules of the  $\alpha_2$ M superfamily must undergo major conformational changes upon activation, and that these events are crucial for their biological activities.

Strikingly,  $\alpha_2$ M/C3-like molecules are not limited to metazoans. Sequence analyses of a number of bacterial genomes have recently identified  $\alpha_2$ M-like genes in several bacteria, most of which are pathogenic species and/or colonize higher eukaryotes [24,25]. This allowed for the identification of two classes of bacterial  $\alpha_2$ Ms, with the most common one carrying the CxEQ motif and being encoded by a gene that is often located juxtaposed to the one coding for Penicillin-Binding Protein 1c (PBP1c). PBPs play key roles in the biosynthesis of peptidoglycan, a three-dimensional mesh that protects the bacterium from differences in osmotic pressure and gives it its shape [26]. This observation led to the suggestion that bacterial  $\alpha_2$ Ms could act in partnership with PBP1c during infection, the former protecting bacteria from proteases, the latter acting in cell wall repair upon potential disruption of the outer membrane and destruction of the peptidoglycan [24]. It is of note that disruption of the outer bacterial membrane could also occur in a non-infectious context, i.e., when members of the same bacterial community compete for nutrients. This suggests that  $\alpha_2$ Ms could be part of a bacterial defense mechanism. A second class of  $\alpha_2$ M, which in many species does not carry the CxEQ motif, was also identified amongst a large number of bacterial strains within an operon coding for four additional lipoproteins [24], but the function of this class of molecule is less clear.

*E. coli* carries both classes of  $\alpha_2$ Ms, and the mechanism of protease inhibition through a thioester-activation mechanism [2] was confirmed for the  $\alpha_2$ M from the PBP1c-related class. This protein was also shown to be modifiable by methylamine and proteases, much like eukaryotic  $\alpha_2$ M [27]. These findings reinforced the suggestion that bacteria, much like their eukaryotic counterparts, could employ  $\alpha_2$ M-like molecules to inhibit target proteases, thus facilitating the infection and colonization processes [24]. Notably, however, eukaryotic  $\alpha_2$ Ms have been reported to exist as dimers and tetramers [2,8], whilst *E. coli*  $\alpha_2$ M is a monomer in solution [27]. This fact could facilitate the characterization of the bacterial form, as well as the detailed comprehension of its functionality. However, it is unlikely that the mechanism of protease targeting by bacterial  $\alpha_2$ M involves physical entrapment, due to its monomeric nature.

Here we report the structural characterization of  $\alpha_2$ M from *Escherichia coli* (henceforth called ECAM, in accordance with [27]) by small angle scattering (SAXS) and electron microscopy techniques in both native, methylamine-treated, and protease-activated forms. The overall shape of this monomeric  $\alpha_2$ M is highly reminiscent of that of C3, for which a high-resolution structure is available. Notably, SAXS experiments indicate that ECAM changes its conformation upon reaction with methylamine, chymotrypsin, or elastase. This modification is reminiscent of that observed for C3 upon activation to yield C3b [19,20,21,22,23] which exposes the thioester region. These results suggest that the mechanism of action of bacterial  $\alpha$ -macroglobulins could involve recognition of proteases from the infected host, or secreted by competing bacterial species, through steps that are associated to a vast structural rearrangement.

## Results and Discussion

### Activated bacterial $\alpha_2$ M highly resembles eukaryotic C3b

The  $\alpha_2$ M from *E. coli* (ECAM) is a 1653-residue molecule that carries a signal peptide, a lipoprotein box immediately following this sequence, and a multi-protease recognition (bait) region

(Fig. 1). Sequence analyses using SMART (<http://smart.embl-heidelberg.de>) suggest the presence of multiple macroglobulin-like (MG) domains as well as a thioester-containing domain (TED), which are hallmarks of eukaryotic proteins of the  $\alpha_2$ M superfamily, including the well-studied C3 molecule. In order to obtain the first structural information of a bacterial  $\alpha_2$ M, we expressed ECAM in its soluble form (i.e., without the signal peptide or lipoprotein sequence) and activated it by treating with methylamine. This procedure yielded homogeneous samples of ECAM that were subsequently analyzed by negative staining electron microscopy employing sodium silico tungstate (pH 7.0, Fig. S1). In total, 51,700 individual particles were selected and aligned against the re-projections of a 30 Å-filtered model of C3 (PDB coordinates 2A73). This projection matching procedure yielded, after 50 cycles, a stable 3D model of ECAM with an estimated resolution between 15 and 20 Å (Fig. S1B). Notably, this 3D model showed clear similarities to the original images obtained by negative staining (Fig. 2A, lines 1 and 3; compare respectively with lines 2 and 4). In order to confirm that our 3D reconstruction was not model-biased, we performed image analysis by a reference-free classification (Figs. S2, S3). Comparison of the final ECAM activated 3D structure (Fig. 2B, gray) with that of C3b, filtered to 15 Å (Fig. 2B, blue), allows for the recognition of a number of key similarities, and one notable difference.

Methylamine-activated ECAM is an elongated molecule with overall dimensions of 140 Å × 80 Å × 80 Å, thus being reminiscent of the structure of C3b, whose dimensions are approximately 140 Å × 80 Å × 70 Å. Analysis of both the raw images and the re-projections of the 3D reconstructions (Fig. 2A and S1) suggest a molecule presenting 3 to 4 main regions of density, which could represent groups of domains, and a considerable level of flexibility. The latter point is also visible in the 3D models of ECAM shown in Fig. 2B, in which the top of the ECAM structure clearly shows two individual regions of electron density (indicated with red arrows). It is of note that only one of these protrusions is present in the filtered structure of C3b (blue, below); it is possible that this region, which corresponds to the C345C domain of C3b's  $\alpha$  chain, is highly flexible in ECAM, and is positioned with two different conformations on the carbon grid, with both conformations being detected in the final structure. Attempts to individually characterize the two conformations were not successful, probably due to the relatively limited number of particles used in the 3D reconstruction (15,000). An alternative explanation to the existence of the two protrusions would be that one of them represents an additional domain present in ECAM but not in its eukaryotic counterparts; this seems unlikely, since sequence comparisons do not indicate the insertion of any large stretches of amino acids that would be required to generate a domain of this size.

Negative staining electron microscopy experiments of the native form were also performed, but a stable 3D model could not be obtained, probably due to a higher flexibility than for the activated form. Thus, in order to expand our study of the conformational changes undertaken by a bacterial  $\alpha$ -macroglobulin during activation, we studied ECAM in native, methylamine-treated, and protease-activated forms by small angle X-ray scattering (SAXS) at physiological pH.

### ECAM changes conformation upon activation

SAXS experiments were performed with four distinct samples: native ECAM, as well as ECAM reacted with methylamine, chymotrypsin, and elastase. All samples were purified by gel filtration chromatography. All activated forms of ECAM migrate faster than the native form in non-denaturing PAGE (Fig. 3A), suggesting that activation induces a conformational change and

confirming the existence of electrophoretically 'fast' forms of bacterial  $\alpha_2$ M [27]. Notably, the transition from 'slow' to 'fast' forms by eukaryotic  $\alpha$ -macroglobulins results in a considerable modification of the overall structure of the dimeric and tetrameric molecules, revealing that the interplay between bait region and thioester cleavage plays key roles in the induction of conformational changes [2].

Scattering patterns were recorded at different ECAM concentrations for all four samples and did not suggest any oligomerization or aggregation events, and are shown in Fig. 3B. The data are represented with the form  $\log I(s)$  versus  $s$  ( $\text{nm}^{-1}$ ), where  $I$  is the measured intensity and  $s$  is the scattering angle. The intensity curve for native ECAM (black, Fig. 3B) shows a distinct side maximum that shifts to higher angles after the protein is reacted with methylamine and suggests that upon activation, ECAM undergoes a conformational change. A qualitatively similar change was also reported for the scattering curves of native and methylamine-treated human  $\alpha_2$ M [11], albeit on a different scale (ECAM is a monomer and human  $\alpha_2$ M a tetramer). In the case of the elastase or chymotrypsin-treated forms, the side maximum is shifted towards higher angles, indicating a compaction of the native structure, which is in agreement with the decrease of the maximum distance ( $D_{\text{max}}$ ) in the  $\rho(r)$  plots (Fig. 3C) from 19 to approximately 16 nm (Table 1). While the  $D_{\text{max}}$  of the native and methylamine-activated forms were similar, it follows from Fig. 3B that the main maximum in the  $\rho(r)$  curve displays a shift from 5.80 for native ECAM to 5.70 nm for the methylamine-treated form. In addition, there were significantly more differences in the range from 10 to 15 nm in the case of the methylamine-activated form with respect to the native form, which suggests a domain rearrangement in line with the increase of the  $R_g$  between both forms (Table 1). Interestingly, this change was more substantial after incubation with proteases, where the maxima were at 5.28 and 5.25 nm for the chymotrypsin and elastase complexes, respectively. Therefore, the modification in  $D_{\text{max}}$ , the shape of the  $\rho(r)$  curve and a modified  $R_g$  all point to the fact that ECAM undergoes a conformational modification after reaction with methylamine, and this change is even more pronounced upon its reaction with proteases. Surprisingly, by employing fluorescence spectroscopy, Doan and Gettins recently concluded that ECAM does not undergo major structural modifications upon treatment with methylamine [27]. The reasons for this discrepancy are unclear, but the results presented here from both EM and SAXS studies clearly show that a conformational modification occurs upon activation.

The slow decline of the  $\rho(r)$  functions at large distances in all samples might suggest that parts of the structure can adopt a second, lowly populated conformation or structural flexibility; this effect is most pronounced for the native and methylamine activated forms (Fig. 3c). However, it should be noted that in the absence of high-resolution models of ECAM our SAXS data alone cannot provide a definitive answer. A more accurate Kratky plot representation revealed some slight structural flexibility that is most pronounced for the native form (Fig. S5). A potential interpretation could be that the C-terminal domain of ECAM can adopt several conformations in solution upon activation. This interpretation is supported by the EM observations/comparison with C3b (Fig. 2B) which show two potential positions for this domain (please see below).

### Conformational modifications of ECAM resemble those of eukaryotic C3 to C3b

Using the scattering data collected on ID14-3, we initially calculated models of native ECAM using GASBOR [28] with

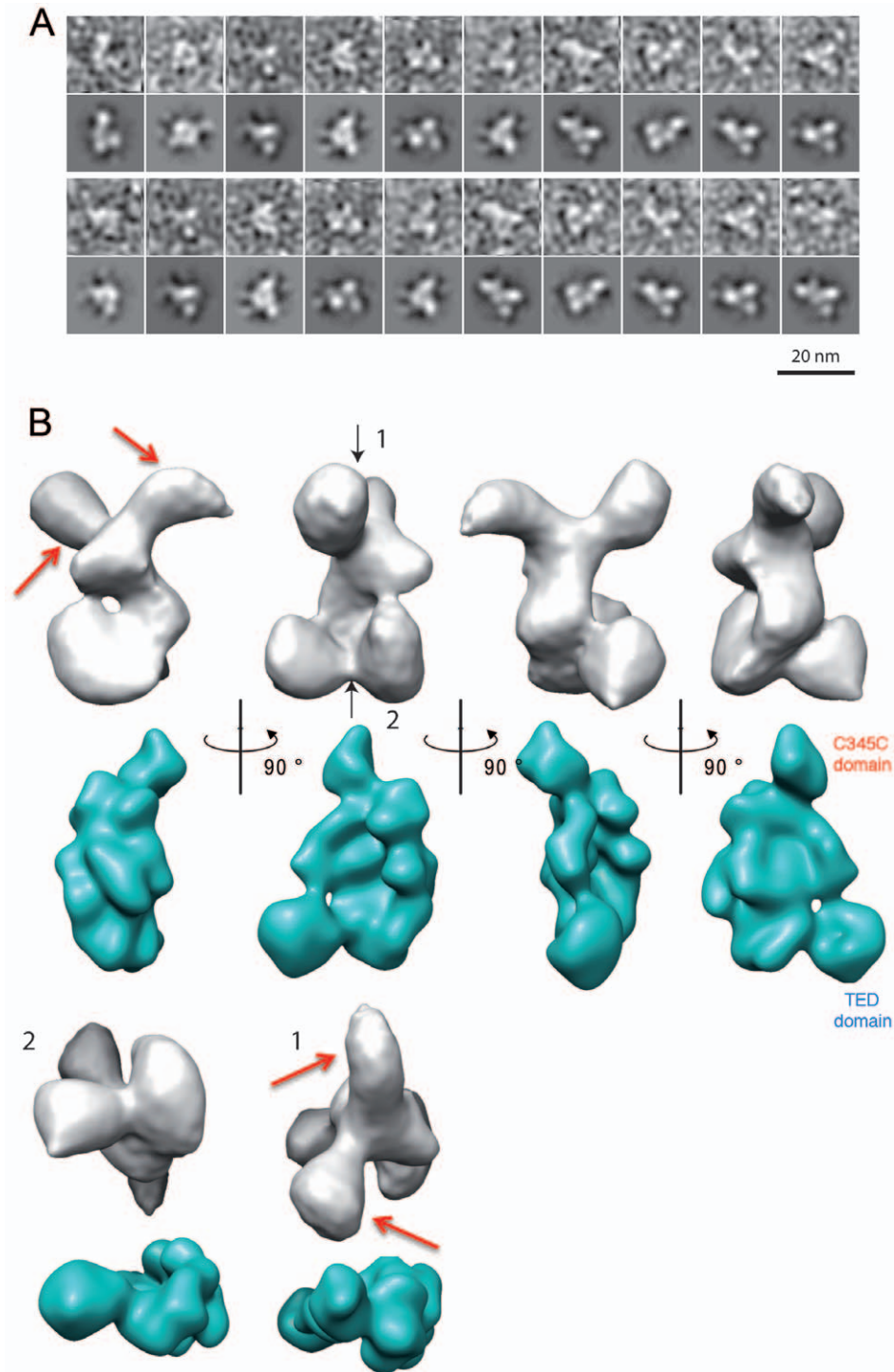


**Figure 2. Electron microscopy reveals that ECAM is an elongated, flexible molecule.** (A) Comparison between raw images, which were low-path filtered at 25 Å (lines 1, 3) and re-projections of the obtained 3D reconstructions (lines 2, 4). (B) Isosurface representations of the 3D reconstruction obtained for the activated form of ECAM (gray) and comparison with the 15 Å filtered structure of C3b (PDB 2I07, blue). For the isosurface representations, an averaged mass density of 0.84 Da/Å<sup>3</sup> and a molecular weight value of 190 kDa were used. Black arrows represent top (1) and bottom (2) views, while the red arrows point to the regions of potentially greatest flexibility.  
doi:10.1371/journal.pone.0035384.g002

default options. After fifteen independent models were generated, they were averaged by DAMAVER [29]. Subsequently, a refined averaged model was calculated using GASBOR by employing a fixed core input file calculated by DAMSTART. The envelope of

the methylamine-activated and protease-reacted forms of ECAM (Figs. 4B, C, D) indicate a clear conformational modification, generating a surface with a pear-like shape in all three cases. Notably, for all three forms, the conformational change generates

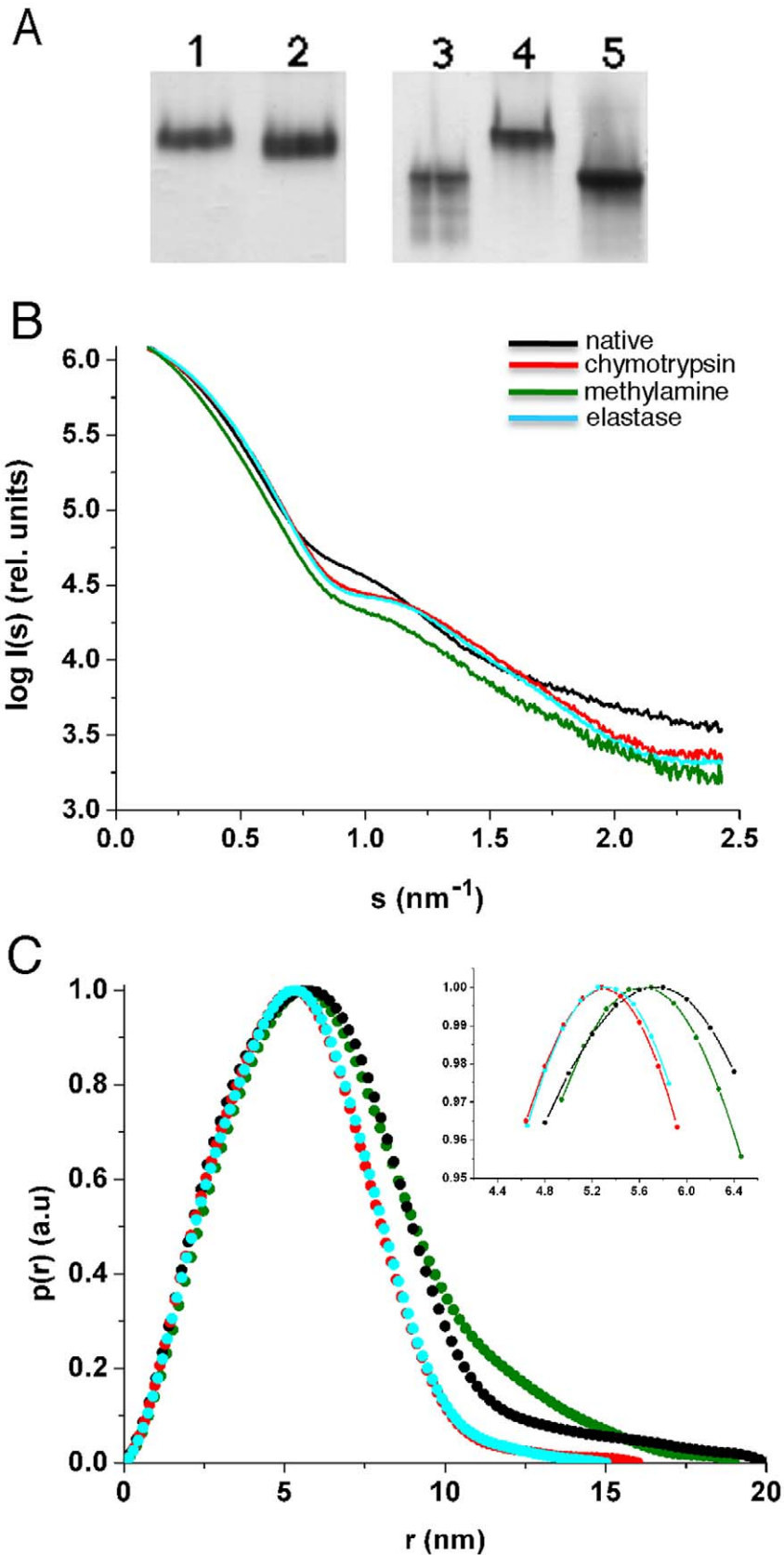


**Figure 3. ECAM shows a change in gel mobility and overall structure upon activation.** (A) Native PAGE showing the migration profile of ECAM. Lanes 1) native molecule; 2) methylamine-treated; 3) after reaction with chymotrypsin; 4) native molecule; 5) after reaction with porcine pancreatic elastase (B) Small-angle X-ray scattering (SAXS) results for native, methylamine-activated, elastase- and chymotrypsin-reacted ECAM. The

radially averaged scattered X-ray intensity was plotted as a function of the momentum transfer  $s$ . Scattering patterns for ECAM in native form (black), after reaction with methylamine (green), elastase (blue) and chymotrypsin (red) were recorded in different concentrations (from 0.5 to 8 mg/mL) but only the curves relating to the highest concentration are shown. Inset, detail of differences in distinct side maxima. (C) Distance distributions  $p(r)$  of native, methylamine-reacted, elastase, and chymotrypsin of ECAM. All curves were normalized. Inset, detail of maxima of  $p(r)$  functions.  
doi:10.1371/journal.pone.0035384.g003

what seems to be a cavity in the central part of the molecule. This feature is reminiscent of the 'MG key ring' reported in structures of C3b and other complement activation factors [19,20,21,22,23,30]. Notably, in the C3 complement system, nucleophilic activation of the inactive thioester induces the TED and CUB domains to move away from the MG key ring, causing the thioester to become exposed; notably, in different structures of C3b, the final position of the TED domain is slightly modified, with respect to the angle that it makes with the rest of the structure [19,20,21,22,23,30]. Thus, in order to explore the possibility that modification of the shape of ECAM from elongated into pear-like could correspond to a conformational change involving clear movement of the TED domain, we manually docked the structures of C3 and C3b onto the SAXS envelopes of native ECAM and methylamine-activated ECAM, respectively. The results are shown in Figs. 5A and 5B, where the envelopes are displayed as a gray mesh, and the structures of C3/C3b as blue ribbons. Results of similar structural comparisons using the program CRYSOLOG [31] are shown in Fig. S4. An initial observation that can be inferred from the abovementioned figures is that both C3 and C3b are similar to ECAM. Interestingly, in the native form of the molecule, one notices additional density for ECAM in a region that corresponds to the C-terminus of C3 (the C345C region). This extra density is also visible in the activated form of the molecule, albeit to a lesser extent.

The views shown in Fig. 5 strongly suggest that the modification in the surface of the activated form of ECAM could correspond to a change in the position of the TED domain, which, in C3b, is located between 75 and 100 Å away from its position in C3 [19,20,21,22,23]. In order to gain further insight into this possibility, we manually fitted the structure of C3b (PDB 2I07, as above) onto the electron microscopy 3D model of methylamine-activated ECAM (Fig. 5C). This analysis reveals two important points. First, it corroborates the location the TED domain (as well as of the MG ring) in the activated form of the bacterial protein. In addition, this analysis suggests that the C-terminal region of C3b could be fitted into two different regions of density; only one was modeled, but the other potential conformation of the C-terminus of ECAM is indicated with red arrows. Thus, both SAXS and EM techniques point to the fact that the C-terminus of ECAM is potentially solvent-exposed and flexible. In eukaryotic  $\alpha_2$ M, the C-terminal, receptor-binding domain is exposed when the molecules are reacted with either methylamine or proteases, thus requiring a conformational modification for solvent accessibility

[4,7,32]. This is also confirmed by the elegant docking of the structure of C3 and C3b onto electron microscopy maps of eukaryotic  $\alpha_2$ M, performed by Janssen and coworkers [20], as well as the recent 4.3 Å crystal structure of methylamine-activated human  $\alpha_2$ M [13]. This suggests that proteins of the  $\alpha_2$ M family share a number of overall structural similarities that include overall conformational modifications upon activation. It is of interest that inhibition of C3b by a Staphylococcal inhibitor protein occurs through the generation of an 'open' conformer of the former, which subsequently blocks formation of the C3 convertase [30], underlining the importance of complex conformational changes not only for C3 function but also for its targeting by pathogens.

The level of circulating  $\alpha_2$ M-protease complexes in humans is low, as a consequence of the recognition of the C-terminus of  $\alpha_2$ M by lipoprotein receptors and their subsequent internalization and degradation. Thus, the C-terminal region of eukaryotic  $\alpha_2$ M plays a key role in its recognition of partner macromolecules, leading to its eventual clearance [1,2,9]. The flexible C-terminal end of ECAM, described here, could also potentially serve as a binding region for partners. This could include PBP1c, whose gene co-occurs with that of  $\alpha$ -macroglobulin in a number of bacterial species [24]. PBP1c is a periplasmic molecule that is anchored to the inner membrane through a single transmembrane region [26,33]. The concerted action of PBP1c and ECAM could favor protection of cell integrity in the presence of foreign proteases [24], potentially through the involvement of a direct interaction between the PBP and the C-terminal region of the  $\alpha$ -macroglobulin. This could reflect a novel bacterial defense mechanism that implicates the action of both protease inhibition and cell wall biosynthesis processes. On the other hand, pathogens have also been shown to encode proteins that mimic components of the complement system in order to manipulate the host inflammatory response [34,35,36]; thus, due to their similarity to C3/C3b, it is conceivable that bacterial  $\alpha$ -macroglobulins could also play yet undefined roles in the disruption of the complement amplification pathway in situations where the outer cell wall is weakened. Either one of these potential mechanisms could represent unexplored targets for the development of novel antibacterials.

## Materials and Methods

### Materials

Porcine pancreatic elastase (PPE) (Fluka Biochemika) was dissolved in 0.2 M Tris-HCl pH 8.0. HisTrap HP, Superdex 200 10/300GL and Mono Q 5/50GL columns were purchased from GE Healthcare. Methylamine hydrochloride was obtained from ACROS Organics.

### Cloning, expression and purification of ECAM

The *yfhm* gene from *Escherichia coli* BL21 was amplified using conventional PCR methods and subsequently cloned into pet15b (Novagen), leading to a construct carrying a N-terminal poly-histidine tag and residues Asp19-Pro1653 of ECAM. The plasmid was transformed into BL21(DE3) and cells were grown in LB broth to an  $OD_{600\text{ nm}}$  of 0.5–0.6 and induced for 3 h at 22°C with 0.5 mM isopropyl B-D-thiogalactoside. Unless otherwise stated buffer A (25 mM HEPES pH 7.5, 0.2 M NaCl) was used in all

**Table 1.** Structural parameters calculated from the models generated from SAXS measurements.

	$R_g$ (nm)	$D_{max}$ (nm)
<b>SAXS</b>		
Native	4.67±0.01	20.0±2.4
Methylamine	5.14±0.03	19.0±1.9
Chymotrypsin	4.14±0.02	16.0±1.9
Elastase	4.14±0.01	15.0±2.0

doi:10.1371/journal.pone.0035384.t001

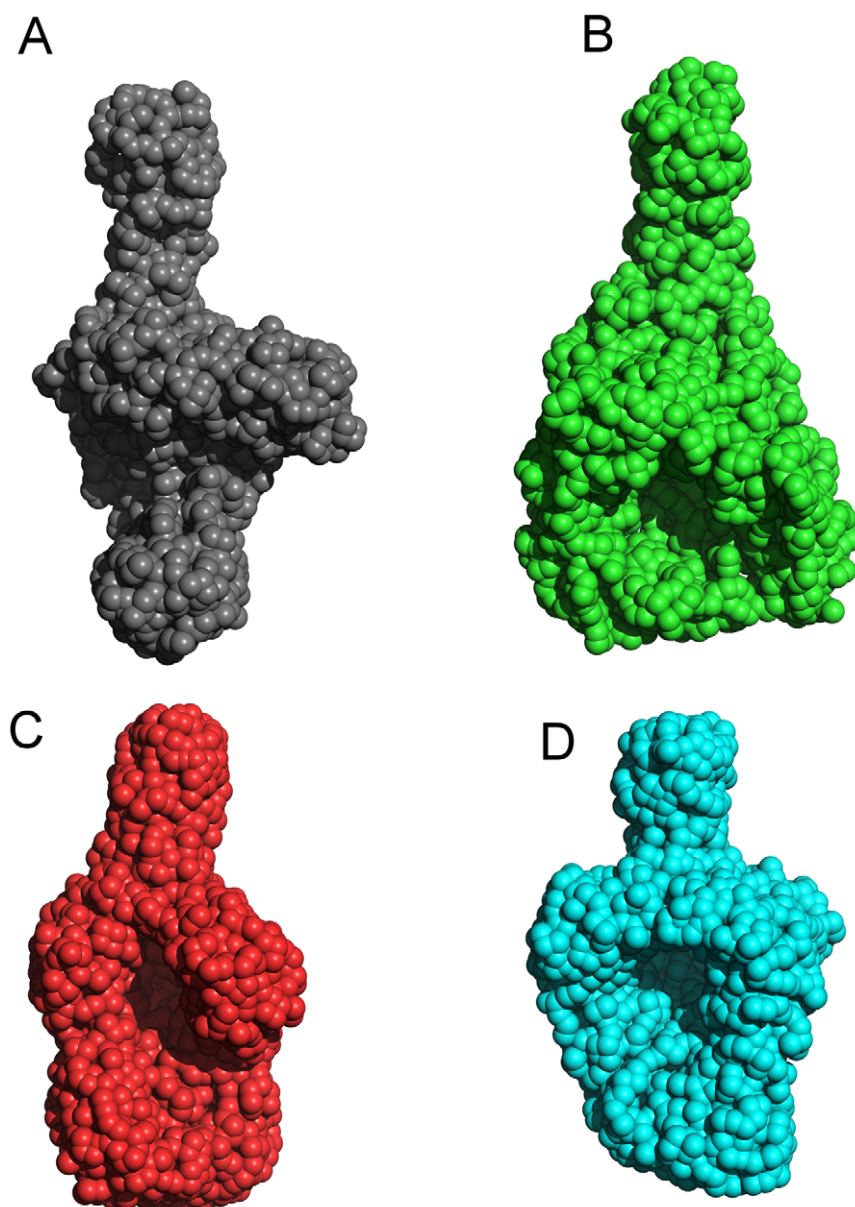


**Figure 4. *Ab initio* models of ECAM generated by SAXS.** Each model results from averaging 10 individual models calculated by the program GASBOR using: (A) native ECAM, (B) methylamine-treated, (C) chymotrypsin-treated, and (D) elastase-treated ECAM. Note the appearance of a central cavity in all of the treated forms of the molecule. GASBOR was used in “user” mode, following default options, except for the total number of residues, which corresponded to total ECAM (1653 residues). The envelopes are based on the  $p(r)$  functions shown on Fig. 3, and the GNOM files generated were used as input for GASBOR. The models are drawn to scale. doi:10.1371/journal.pone.0035384.g004

purification steps. After centrifugation of the cellular suspension at 5,000 g for 20 min at 4°C, the pellet was resuspended in buffer A complemented with anti-proteases leupeptin (0.5  $\mu\text{g}/\text{mL}$ ), aprotinin (0.7  $\mu\text{g}/\text{mL}$ ), PMSF (1.0 mM) and pepstatin (0.7  $\mu\text{g}/\text{mL}$ ). The lysate was obtained by sonication, centrifuged for removal of debris at 40,000 g for 40 min (4°C), and subsequently loaded onto a 5 mL HisTrap column in buffer A complemented with 50 mM imidazole. Protein was eluted with a single 250 mM imidazole step, and fractions were dialyzed overnight at 4°C against 25 mM HEPES pH 7.5, 10 mM NaCl. ECAM-containing fractions were subsequently loaded onto a Mono Q column equilibrated in the dialysis buffer and eluted with a linear gradient to 0.5 M NaCl. ECAM was further purified by gel filtration chromatography using

a Superdex 200 column equilibrated in buffer A. The central fractions of the peak corresponding to ECAM were pooled and concentrated to 10 mg/mL.

#### Preparation of activated forms of ECAM

Methylamine activation experiments were performed by incubating pure ECAM with 200 mM methylamine hydrochloride and 200 mM Tris-HCl pH 8.0 for 2 h at 25°C and subsequently subjecting the sample to gel filtration chromatography as described above. The central fractions of the peak were pooled and concentrated to 10 mg/mL.

The reactions with elastase and chymotrypsin were carried out using the same protocol. A 1:1 molar ratio of protease:ECAM was

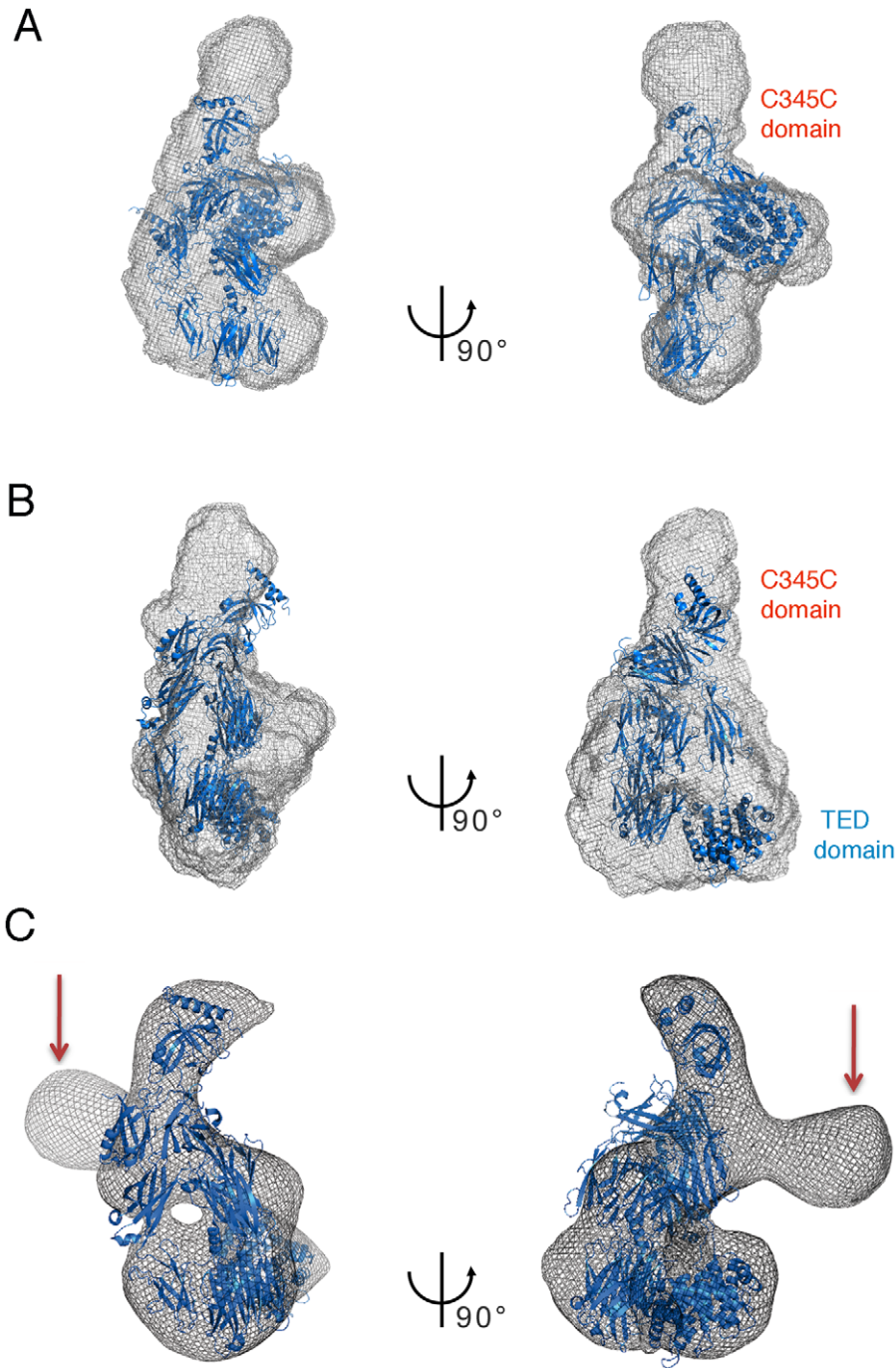


**Figure 5. The structures of both native and activated forms of ECAM resemble those of C3 and C3b.** Surface representations of ECAM in native (A) and methylamine-activated (B) states based on SAXS measurements. Structures of C3 (PDB 2A73) and C3b (PDB 2I07, in blue) were modeled manually into the ECAM *ab initio* SAXS models. Note that the difference in position of the C3/C3b TED (thioester-containing) domain can be well accounted for in the SAXS envelopes of both native (A) and methylamine-activated (B) forms of ECAM. (C) The X-ray structure of C3b (PDB 2I07) was manually fitted into the 3D EM envelope of the activated ECAM. The size of the macromolecule as well as the MG ring and the TED domain are in comparable positions. The unoccupied density, shown with red arrows, indicates the different potential position of the C-terminus domain and indicates high flexibility in this region. The lack of sequence similarity between the C-terminal domain of ECAM and C3b (Fig. S6) could also account for the differences observed.

doi:10.1371/journal.pone.0035384.g005

incubated at 37°C for 10 minutes, and the reaction was stopped with 1 mM PMSF, and subsequently injected on a gel filtration column; only the central fractions of the peak were used for further experiments.

#### Small-angle X-ray Scattering

Measurements were recorded at the ID14-3 beamline of the European Synchrotron Radiation Facility (Grenoble, France). Prior to data collection a scattering curve of bovine serum albumin

reference solution (5.2 mg/mL) was recorded. Experiments were performed at concentrations of 8.0 mg/mL for native ECAM, 6.4 mg/mL for the methylamine-activated form, 7.6 mg/mL for elastase-incubated ECAM and 6.1 mg/mL for the chymotrypsin-reacted ECAM. Between measurements, scattering from a buffer sample was recorded, and these data were subsequently subtracted from the respective sample curves. No radiation damage was observed during the ten 10 second exposure frames and all data were recorded at 25°C. Data were treated following default parameters of the PRIMUS software package [37]. The radius of gyration  $R_g$  and the forward scattering value  $I(0)$  were estimated using the Guinier approximation [38]. Both parameters, as well as the maximum particle dimension  $D_{max}$ , were also calculated by the GNOM software [39]. *Ab initio* models of ECAM were generated using GASBOR [28]. A final average model was generated from 15 independent models using DAMAVER through their pairwise superposition [29].

**Electron microscopy** - Activated ECAM at a concentration of 0.05 mg/mL was first applied to the clean side of carbon on mica (carbon/mica interface) and negatively stained with 1% (w/v) sodium silico tungstate [40]. A grid was placed on top of the carbon film, and subsequently air-dried. Images were taken under low dose conditions with a Polara microscope (FEI Eindhoven, The Netherlands) operating at 300 kV and a nominal magnification of 59,000 $\times$  with a Gatan CCD camera (USC 4000) (pixel size at the specimen level: 2 Å; defocus values ranging from 1.5 to 3  $\mu$ m). A total of 51,700 particles were selected using a semi-automatic particle selection procedure with the EMAN boxer routine [41] and extracted into 100 $\times$ 100 pixel boxes. The images were CTF-corrected with CTFFIND3 [42] and Bsoft [43] and low-path-filtered to 25 and 10 Å. Due to the inherent flexibility of ECAM, only 15,000 particles were used to calculate the final 3D model, since the inclusion of a larger number of particles decreased the resolution.

### Image processing

A SPIDER [44]-based projection matching analysis using an initial 3D model calculated from the related C3 structure (PDB 2A73 filtered at 30 Å) was performed. A total number of 800 equally spaced re-projections (5 degrees sampling) and 50 cycles were used to obtain the final 3D reconstruction (the orientation parameters of the raw images and 3D reconstruction were stable). Each cycle consisted of model re-projections, alignment using the 25 Å low-path-filtered stack file, and 3D reconstructions using the 10 Å low-path-filtered stack file. Only the best 15,000 images (cross correlation criteria) were used during each cycle of projection matching. The resolution of the active form of the ECAM was found to be between 15 and 20 Å (0.3 and 0.5 Fourier-shell correlation criteria, respectively; Fig. S1B). A manual fit the C3b convertase (pdb 2I07) was performed using PYMOL.

### Reference-free image classification

*Ab-initio* image classification was performed by using the IMAGIC software (ImageScience). After an initial centering step based on the average of all images, a multivariate statistical analysis (MSA) was performed by using a set of 69 eigen-images. The EM raw images were divided by similarity into 150 classes and the class averages were used to re-align/re-center the images; the above process was iterated 3 times, resulting in the classes presented in Fig. S2B. These classes were aligned against 196 equally distributed re-projections (every 10 degrees) of our

reconstruction (Fig. S2A). The result is show in Fig. S3. Rows labeled 1 show the re-projections of our reconstruction whereas rows labeled 2 show the *ab initio* classes averages (same images as in panel S2b). For each re-projection, the corresponding *ab initio* calculated classes are very similar, confirming our 3D reconstruction.

### Supporting Information

**Figure S1** A- Typical electron microscopy field of view obtained on SST negatively stained ECAM. B- Fourier shell correlation obtained by splitting the 15,000 images into halves in order to calculate two independent reconstructions (Yang et al., 2003). (JPG)

**Figure S2** Comparison between equally distributed re-projections (every 10 degrees; 196) of the EM 3D reconstruction (A) and the *ab-initio* obtained classes (150) (B). (JPG)

**Figure S3** Alignment of the 150 classes (Fig. S2B) against the 196 re-projections of our 3D reconstruction (Fig. S2A). The re-projections are shown in the rows labeled "1", and for each re-projection, the corresponding aligned classes are shown as a column (part 2). (JPG)

**Figure S4** Comparison of the SAXS data for both native and methylamine-activated ECAM with the crystal structures of C3 and C3b, respectively, using the program CRY SOL. Both fits are relatively good at low angles, indicating that the overall shapes (i.e., radii of gyration) are similar. (TIF)

**Figure S5** Kratky plot of SAXS experiments, which indicates that native ECAM is the form that displays the highest amount of flexibility. (TIF)

**Figure S6** Alignment of the C-terminal sequences of ECAM and C3, performed with the MUSCLE server. Identical residues are indicated with red boxes, and similar amino acids in gray. The CxEQ motif is indicated with diamonds. The two regions display 30% sequence similarity. Reference for FigureS6: Yang S, Yu X, Galkin VE, Egelman EH (2003). Issues of resolution and polymorphism in singleparticle reconstruction. J. Struct. Biol. 144, 162–171. (PDF)

### Acknowledgments

The authors wish to thank the IBS Block allocation group SAXS beamtime on the ID14-3 beamline of the European Synchrotron Radiation Facility (ESRF, Partnership for Structural Biology, PSB), and Adam Round for help with SAXS data collection. Daphna Fenel (PSB electron microscopy platform) and Dr. Wai-Li Ling are acknowledged for preliminary negative staining experiments. The Polara microscope is part of the IBS Structural Biology and Dynamics GIS-IBISA- labeled platform.

### Author Contributions

Conceived and designed the experiments: DN FG GS AD. Performed the experiments: DN LE VJ FG GS. Analyzed the data: DN FG GS AD. Contributed reagents/materials/analysis tools: LE FG GS. Wrote the paper: DN AD.

## References

- Armstrong PB (2006) Proteases and protease inhibitors: a balance of activities in host-pathogen interaction. *Immunobiology* 211: 263–281.
- Sottrup-Jensen L (1989) Alpha macroglobulins: structure, shape, and mechanism of proteinase complex formation. *J Biol Chem* 264: 11539–11542.
- Kolodziej SJ, Wagenknecht T, Strickland DK, Stoops JK (2002) The three-dimensional structure of the human  $\alpha_2$ -macroglobulin dimer reveals its structural organization in the tetrameric native and chymotrypsin a 2-macroglobulin complexes. *J Biol Chem* 277: 28031–28037.
- Qazi U, Kolodziej SJ, Gettins PGW, Stoops JK (2000) The structure of the C949S mutant human  $\alpha_2$ -macroglobulin demonstrates the critical role of the internal thiol esters in its proteinase-entrapping structural transformation. *J Struct Biol* 131: 19–26.
- Boisset N, Taveau J-C, Ponchon F, Lamy J (1996) Similar architectures of native and transformed human  $\alpha_2$ -macroglobulin suggest the transformation mechanism. *J Biol Chem* 271: 25762–25769.
- Arakawa H, Nishigai M, Ikai A (1989)  $\alpha_2$ -macroglobulin traps a proteinase in the midregion of its arms. *J Biol Chem* 264: 2350–2356.
- Delain E, Barray M, Trapon-Bretaudiere J, Ponchon F, Maryen P, et al. (1988) The molecular organization of human  $\alpha_2$ -macroglobulin. *J Biol Chem* 263: 2981–2989.
- Delain E, Pochon F, Barray M, van Leuven F (1992) Ultrastructure of alpha 2-macroglobulins. *Electron Microsc Rev* 5: 231–281.
- Jenner L, Husted L, Thirup S, Sottrup-Jensen L, Nyborg J (1998) Crystal structure of the receptor-binding domain of  $\alpha_2$ -macroglobulin. *Structure* 6: 595–604.
- Boisset N, Penczek P, Ponchon F, Frank J, Lamy J (1993) Three-dimensional architecture of human  $\alpha_2$ -macroglobulin transformed with methylamine. *J Mol Biol* 232: 522–529.
- Osterberg R, Malmensten B (1984) Methylamine-induced conformational change of  $\alpha_2$ -macroglobulin and its zinc(II) binding capacity. *Eur J Biochem* 143: 541–544.
- Branegard B, Osterberg R, Sjoberg B (1982) Small-angle X-ray scattering study of the interaction between human  $\alpha_2$ -macroglobulin and trypsin. *Eur J Biochem* 122: 663–666.
- Marrero A, Duquerroy S, Trapani S, Goulas T, Guevara T, et al. (2012) The crystal structure of human  $\alpha_2$ -macroglobulin reveals a unique molecular cage. *Angew Chem Int Ed Engl* e-print.
- Gros P, Milder FJ, Janssen BJC (2008) Complement driven by conformational changes. *Nat Rev Immunol* 8: 48–58.
- Sahu A, Lambris JD (2001) Structure and biology of complement protein C3, a connecting link between innate and acquired immunity. *Immun Rev* 180: 35–48.
- Kirkitadze MD, Barlow PN (2001) Structure and flexibility of the multiple domain proteins that regulate complement activation. *Immun Rev* 180: 146–161.
- Janssen BJC, Huizinga EG, Raaijmakers HC, Roos A, Daha MR, et al. (2005) Structures of complement component C3 provide insights into the function and evolution of immunity. *Nature* 437: 505–511.
- Freslund F, Jenner L, Husted LB, Nyborg J, Andersen GR, et al. (2006) The structure of bovine complement component 3 reveals the basis for thioester function. *J Mol Biol* 361: 115–127.
- Alcorlo M, Martinez-Barricarte R, Fernandez FJ, Rodriguez-Gallego C, Round A, et al. (2011) Unique structure of iC3b resolved at a resolution of 24 Å by 3D-electron microscopy. *Proc Natl Acad Sci USA* 108: 13236–13240.
- Janssen BJC, Christodoulidou A, McCarthy A, Lambris JD, Gros P (2006) Structure of C3b reveals conformational changes that underlie complement activity. *Nature* 444: 213–216.
- Nishida N, Walz T, Springer TA (2006) Structural transitions of complement component C3 and its activation products. *Proc Natl Acad Sci USA* 103: 19737–19742.
- Wiesmann C, Katschke Jr. KJ, Yin J, Helmy KY, Steffek M, et al. (2006) Structure of C3b in complex with CR1g gives insights into regulation of complement activation. *Nature* 444: 217–220.
- Baxter RHG, Chang C-I, Chelliah Y, Blandin S, Levashina EA, et al. (2007) Structural basis for conserved complement factor-like function in the antimalarial protein TEPI. *Proc Natl Acad Sci USA* 104: 11615–11620.
- Budd A, Blandin S, Levashina E, Gibson TJ (2004) Bacterial  $\alpha_2$ -macroglobulins: colonization factors acquired by horizontal gene transfer from the metazoan genome? *Genome Biol* 5: R38.
- Kantyka T, Rawlings ND, Potempa J (2010) Prokaryote-derived protein inhibitors of peptidases: a sketchy occurrence and mostly unknown function. *Biochimie* 92: 1644–1656.
- Mattei P-J, Neves D, Dessen A (2010) Bridging cell wall biosynthesis and bacterial morphogenesis. *Curr Opin Struct Biol* 20: 749–766.
- Doan N, Gettins GW (2008) Alpha-macroglobulins are present in some Gram-negative bacteria: characterization of the alpha2-macroglobulin from *Escherichia coli*. *J Biol Chem* 283: 28747–28756.
- Svergun DI, Petoukhov MV, Koch MH (2001) Determination of domain structure of proteins from X-ray solution scattering. *Biophys J* 80: 2946–2953.
- Volkov VV, Svergun DI (2003) Uniqueness of ab initio shape determination in small-angle scattering. *Journal of Applied Crystallography* 36: 860–864.
- Chen H, Ricklin D, Hammel M, Garcia BL, McWhorter WJ, et al. (2010) Allosteric inhibition of complement function by a staphylococcal immune evasion protein. *Proc Natl Acad Sci USA* 107: 17621–17626.
- Svergun D, Barberato C, Koch MHJ (1995) CRYSOLE - A program to evaluate X-ray solution scattering of biological macromolecules from atomic coordinates. *J Appl Cryst* 28: 768–773.
- Carlsson-Bostedt L, Moestrup SK, Gliemann J, Sottrup-Jensen L, Stigbrand T (1988) The different conformational states of pregnancy zone protein identified by monoclonal antibodies. *J Biol Chem* 263: 6738–6741.
- Schiffner G, Holtje JV (1999) Cloning and characterization of PBP1c, a third member of the multimodular class A penicillin-binding proteins of *Escherichia coli*. *J Biol Chem* 274: 32031–32039.
- Kotwal GJ (2000) Poxvirus mimicry of complement and chemokine system components. *Immunol today* 21: 243–248.
- Murthy KHM, Smith SA, Ganesh VK, Judge KW, Mullin N, et al. (2001) Crystal structure of a complement control protein that regulates both pathways of complement activation and binds heparan sulfate proteoglycans. *Cell* 104: 301–311.
- Rooijackers SHM, van Strijp JAG (2007) Bacterial complement evasion. *Mol Immunol* 44: 23–32.
- Konarev PV, Volkov VV, Sokolova AV, Koch MHJ, Svergun DI (2003) PRIMUS: a Windows PC-based system for small-angle scattering data analysis. *Journal of Applied Crystallography* 36: 1277–1282.
- Guinier A, Fournet G (1955) Small angle scattering of X-rays. New York: Wiley.
- Svergun D (1992) Determination of the regularization parameter in indirect-transform methods using perceptual criteria. *Journal of Applied Crystallography* 25: 495–503.
- Trapani S, Abergel C, Gutsche I, Horcajada C, Fita I, et al. (2006) Combining experimental data for structure determination of flexible multimeric macromolecules by molecular replacement. *Acta Cryst Sect D* 62: 467–475.
- Ludtke SJ, Baldwin PR, Chiu W (1999) EMAN: semiautomated software for high-resolution single-particle reconstructions. *J Struct Biol* 128: 82–97.
- Mindell JA, Grigorieff N (2003) Accurate determination of local defocus and specimen tilt in electron microscopy. *J Struct Biol* 142: 334–347.
- Heymann JB, Cardone G, Winkler DC, Steven AC (2008) Computational resources for cryo-electron tomography in Bsoft. *J Struct Biol* 161: 232–242.
- Frank J, Radermacher M, Penczek P, Zhu J, Li Y, et al. (1996) SPIDER and WEB: processing and visualization of images in 3D electron microscopy and related fields. *J Struct Biol* 116: 190–199.